
DreamScene4D: Dynamic Multi-Object Scene Generation from Monocular Videos

Wen-Hsuan Chu[†], Lei Ke[†], Katerina Fragkiadaki

Carnegie Mellon University

{wenhsuac,leik,katef}@cs.cmu.edu

<https://dreamscene4d.github.io/>

Abstract

Existing VLMs can track in-the-wild 2D video objects while current generative models provide powerful visual priors for synthesizing novel views for the highly under-constrained 2D-to-3D object lifting. Building upon this exciting progress, we present DreamScene4D, the first approach that can generate three-dimensional dynamic scenes of multiple objects from monocular in-the-wild videos with large object motion across occlusions and novel viewpoints. Our key insight is to design a “*decompose-then-recompose*” scheme to factorize both the whole video scene and each object’s 3D motion. We first decompose the video scene by using open-vocabulary mask trackers and an adapted image diffusion model to segment, track, and amodally complete the objects and background in the video. Each object track is mapped to a set of 3D Gaussians that deform and move in space and time. We also factorize the observed motion into multiple components to handle fast motion. The camera motion can be inferred by re-rendering the background to match the video frames. For the object motion, we first model the object-centric deformation of the objects by leveraging rendering losses and multi-view generative priors in an object-centric frame, then optimize object-centric to world-frame transformations by comparing the rendered outputs against the perceived pixel and optical flow. Finally, we recombine the background and objects and optimize for relative object scales using monocular depth prediction guidance. We show extensive results on the challenging DAVIS, Kubric, and self-captured videos, detail some limitations, and provide future directions. Besides 4D scene generation, our results show that DreamScene4D enables accurate 2D point motion tracking by projecting the inferred 3D trajectories to 2D, while never explicitly trained to do so.

1 Introduction

Videos are result of entities moving and interacting in 3D space and time, projected from camera viewpoints. Generating 4D scenes from 2D monocular videos has wide applicability across multiple end tasks, such as 3D video perception, or creating digital avatars, assets, and virtual environments that accurately mirror the real world for graphics or robotics [14, 35]. This task, referred to as video-to-4D, aims to infer the 3D structure and motion of video objects in dynamic 3D scenes across occlusions and unseen camera viewpoints, while preserving the spatial-temporal consistency and reality to the 2D observation. However, the task has remained unsolved for many years due to its under-constrained nature, especially in a casual setup with time-varying geometry and limited 3D supervision from in-the-wild videos.

Despite the remarkable progress in 4D generation, existing works mostly focus on text-to-4D [45, 2, 52, 24, 1] or image-to-4D [63, 42, 56, 65] setups, which take a single text or image as input to single 4D object creation. Several works [15, 12, 42, 31, 59, 60] explore the video-to-4D setup,

[†]Equal contribution

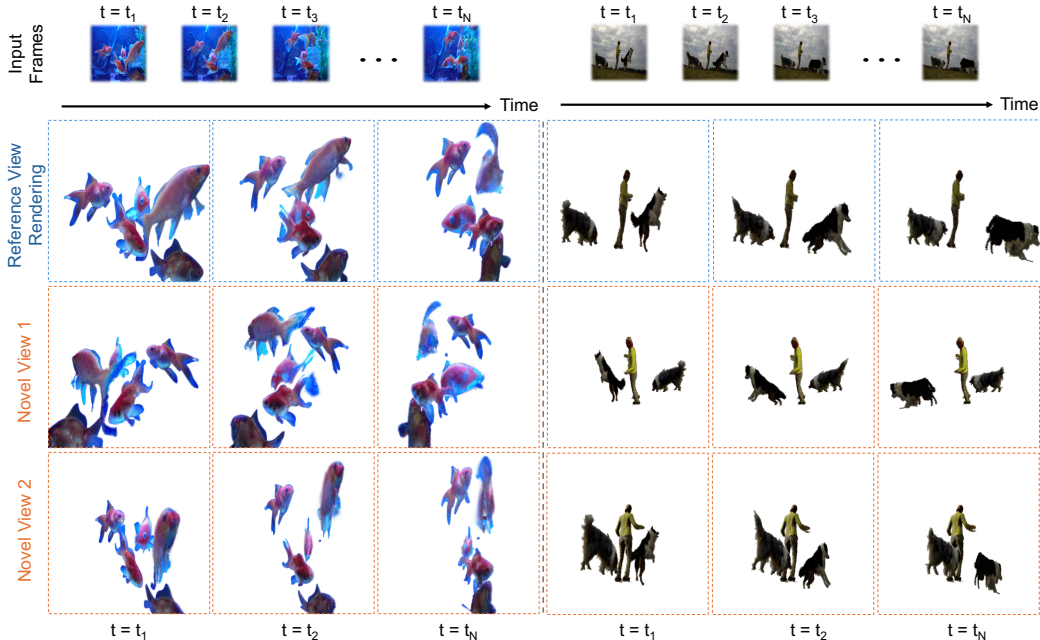


Figure 1: **DreamScene4D** extends video-to-4D generation to multi-object videos with fast motion. We present rendered images from diverse viewpoints at different timesteps using DAVIS [36] videos with multiple objects and large motions.

but they can only handle object-centric videos with a single object of small movement. This limits their practical real-world usage where input videos depicting real-world complex scenes containing multiple dynamic objects with fast motions, as illustrated in Figure 4.

In this paper, we propose DreamScene4D, the first video-to-4D scene generation approach to produce realistic 4D scene representation from a complex multi-object video with large object motion or deformation. DreamScene4D proposes a “decompose-then-recompose” strategy. First, the objects and background in the video are tracked and segmented. As occlusions are common in multi-object videos, we adapt a diffusion model to temporally inpaint the background and potentially occluded object tracks, then independently lift them to 3D using 3D Gaussian representation.

In DreamScene4D, the 3D motion is factorized into three components: 1) camera motion, 2) object-centric deformations, and 3) an object-centric to world frame transformation. This factorization greatly improves the stability of the motion optimization process by leveraging powerful pre-trained 3D diffusion and 2D tracking priors [26, 48]. The camera motion can be estimated by re-rendering the static background Gaussians to match the video frames. Finally, we re-compose the background and dynamic objects for joint fine-tuning and optimize the scale for each lifted object using predicted monocular depth to place them into a common coordinate frame.

We show the 4D renderings at various timesteps and diverse viewpoints of DreamScene4D using challenging monocular videos from DAVIS [36] in Figure 1. DreamScene4D achieves significant improvements compared to the existing SOTA video-to-4D approaches [42, 15] on DAVIS, Kubric [13], and our self-captured videos (Figures 4). To evaluate the quality of the learned Gaussian motions, we measure the 2D endpoint error (EPE) of the inferred 3D motion trajectories across occlusions and reveal that our approach not only enables point tracking in the visible views but also empowers accurate point tracking in the synthesized novel views.

2 Related Work

Video-to-4D Generation Recent advancements in generative diffusion models spark a series of 4D generation works [45, 42], which typically use score distillation sampling (SDS) [37] loss by large-scale pretrained diffusion models [44] to synthesize full 4D representations of objects from single text [45, 2, 24, 1], image [56, 65], or a combination of both [63]. Existing video-to-4D generation works [42, 15, 12, 31, 59, 60] mostly combine SDS with existing 3D or 4D representations

like DyNeRF [23] or 4D Gaussians [50], and can only take simple videos with single object of small motion as input. In contrast, owing to our proposed scene decoupling and motion factorization schemes, DreamScene4D is the first approach to generate complicated 4D scenes and synthesize their arbitrary novel views by taking real-world videos of multi-object scenes.

Video-to-4D Reconstruction Dynamic 3D reconstruction is another related research line, which extends static 3D reconstruction to dynamic scenes. Dynamic NeRF-based methods [38, 32, 23] extend NeRF [30] to dynamic scenes, typically using grid or voxel-based representations [27, 4, 25], or learning a deformation field [4, 11] that models the dynamic portions of an object or scene. Dynamic Gaussian Splatting [29] extends 3D Gaussian Splatting [19], where scenes are represented as 4D Gaussians and show faster convergence than NeRF-based approaches. However, these 4D scene reconstruction works [29, 50, 57] typically take a large number of synchronized multi-view video data as input instead of un-posed monocular videos with insufficient parallax, which necessitate precise calibration of multiple cameras and constrains their potential real-world applicability. Different from these works [33, 50] on mostly reconstructing the visible regions of the dynamic scene, DreamScene4D can 360° synthesize novel views for multiple objects of the scene, including the occluded/invisible regions.

Video Scene Completion Existing video-to-4D scene generation works [42, 31, 59, 60] usually simplify the input video by assuming a non-occluded and slow-moving object while real-world videos with multiple dynamic objects inevitably contain occlusions. Thus, we also perform video amodal completion in our works to inpaint the occluded video objects or background regions of the video. Compared to existing image/video scene completion works [61, 10, 17, 66], the video completion in DreamScene4D is not limited to small close-world categories and only serves as an intermediate step for the 4D video scene completion. Instead, we adapt large-scale pre-trained diffusion models SD-Inpaint [44] with temporal layers for video scene completion due to its rich prior on objects.

3 Approach

To generate dynamic 4D scenes of multiple objects from a monocular video input, we propose DreamScene4D, which takes Gaussian Splatting [19, 50] as the 4D scene representation and leverages powerful pre-trained models to generalize to diverse zero-shot settings.

Our approach follows the “decompose-then-compose” principle to handle complex multi-object scenes. As depicted in Figure 2, given a monocular video of multiple objects, we first segment and track [43, 18, 8] each 2D video object in-the-wild and recover the appearance of the occluded regions of each object and the background with realistic temporal consistency (Section 3.1). Next, we decompose the scene into multiple amodal objects and use SDS with diffusion priors to extract a 3D Gaussian representation of each object. We optimize the deformation of 3D Gaussians for dynamic objects under 2D constraints by re-rendering the video frames and factorizing the motion into three components (Figure 3): the object-centric motion, a global translation, and the camera motion, which greatly improves the stability and quality of the optimization (Section 3.2). Finally, guided by monocular depth prediction of the scene, we compose each individually optimized object to form a complete 4D scene representation of the monocular video (Section 3.3).

3.1 Video Scene Decomposition and Completion

We first adopt zero-shot mask trackers [43, 18, 8] to segment and track objects in the monocular video when GT object masks are not provided. From the monocular video and associated object tracks (with potential occlusions), we amodally complete each object track in a temporally consistent manner before lifting it to 3D as in Figure 2.

To achieve zero-shot object appearance recovery for occluded regions of individual object tracks, we build off of SD-Inpaint, an adapted Stable Diffusion model [44] with rich image inpainting priors, and extend it to videos for amodal video completion. When directly adopting SD-Inpaint to complete the objects in videos, the inpainting results suffer from obvious temporal artifacts. Therefore, we propose two extensions to SD-Inpaint to overcome this problem without further training or finetuning.

Spatial-Temporal Self-Attention A common technique for extending Stable Diffusion-based models for video generation editing inflates the spatial self-attention layers to additionally attend across frames without changing the pre-trained weights [51, 20, 5, 39]. Similar to [5], we inject tokens from

adjacent frames during self-attention to enhance inpainting consistency. Specifically, the self-attention operation can be denoted as:

$$Q = W_Q z_t, K = W_K [z_{t-1}, z_t, z_{t+1}], V = W_V [z_{t-1}, z_t, z_{t+1}], \quad (1)$$

where $[\cdot]$ represents concatenation, z_t is the latent representation of frame t , and W_Q, W_K , and W_V denote the (frozen) projection matrices that project inputs to queries, keys, and values.

Latent Consistency Guidance While inflating the self-attention layers allows the diffusion model to attend to and denoise multiple frames simultaneously, it does not ensure that the inpainted video frames are temporally consistent. To solve this issue, we take inspiration from previous works that perform test-time optimization while denoising for structured image editing [34] and panorama generation [22] and explicitly enforce the latents during denoising to be consistent.

Concretely, we follow a two-step process for each denoising step for noisy latent z^τ at denoising timestep τ to latent $z^{\tau-1}$. For each noisy latent z_t^τ at frame t , we compute the fully denoised latent z_t^0 and its corresponding image \hat{I}_t directly in one step. To encourage the latents of multiple frames to become semantically similar, we freeze the network and only update z^τ :

$$\hat{z}^\tau = z^\tau - \eta \nabla_z \mathcal{L}_c, \quad (2)$$

where η determines the size of the gradient step and \mathcal{L}_c is a similarity loss, i.e., CLIP feature loss or the SSIM between pairs of \hat{I}_t . After this latent optimization step, we take \hat{z}^τ and predict the added noise $\hat{\epsilon}^\tau$ using the diffusion model to compute $z^{\tau-1}$ as:

$$z^{\tau-1} = \sqrt{\alpha_{t-1}} \left(\frac{\hat{z}^\tau - \sqrt{1 - \alpha_t} \hat{\epsilon}^\tau}{\sqrt{\alpha_t}} \right) + \sqrt{1 - \alpha_{t-1}} \hat{\epsilon}^\tau, \quad (3)$$

where α_t is the noise scaling factor defined in DDIM [46].

3.2 3D Dynamic Object Generation from Videos

Next, we aim to generate 4D objects based on the amodally completed 2D videos from Section 3.1. This requires lifting each video object and the background into 3D and modeling its motion.

3.2.1 Object-Centric 3D Lifting from Global Frame

After decomposing the scene into individual amodal object tracks, we use Gaussians Splatting [19] with SDS to lift these 2D objects to 3D. For each object track, instead of directly lifting the 3D object on the original video frame, where object areas are small, we take the cropped and scaled first frame \tilde{I}_1 of the new object-centric video to optimize the static 3D Gaussians representation with both the photometric rendering loss ($t = 1$ in Eq. 5) on the input reference view and score distillation sampling (SDS) loss [37], similar to the process described in [48]:

$$\nabla_\phi \mathcal{L}_{\text{SDS}}^{\text{img}} = \mathbb{E}_{\tau, \epsilon, p} \left[w(\tau) \left(\epsilon_\theta \left(\hat{I}_1^p; \tau, \tilde{I}_1, p \right) - \epsilon \right) \frac{\partial \hat{I}_1^p}{\partial \phi} \right], \quad (4)$$

where $w(\tau)$ is the SDS weighting function at denoising timestep τ , $\phi(\cdot)$ represents the Gaussian rendering function, \hat{I}_1^p is the rendered image, $\epsilon_\theta(\cdot)$ is the predicted noise from a diffusion prior, and ϵ is the added noise. We take the superscript p to represent an arbitrary camera pose.

3.2.2 Modeling Complex 3D Motions via Motion Factorization

To estimate the motion of the first-frame lifted 3D Gaussians $\{G_1^{\text{obj}}\}$, a straightforward solution is to model the object dynamics by optimizing the deformation of the 3D Gaussians in the total T world frame of the video. However, this approach falls short in videos with large object motion, as the rendering loss yields insignificant gradients until there is an overlap between the deformed Gaussians in the re-rendered frames and the objects in the video frames. Thus, we propose to decompose the dynamics into three components, and independently model them: **1)** object-centric motion, modeled using a learnable deformation network; and **2)** the object-centric to world frame transformation, represented by a set of 3D displacements vectors and scaling factors; and **3)** camera

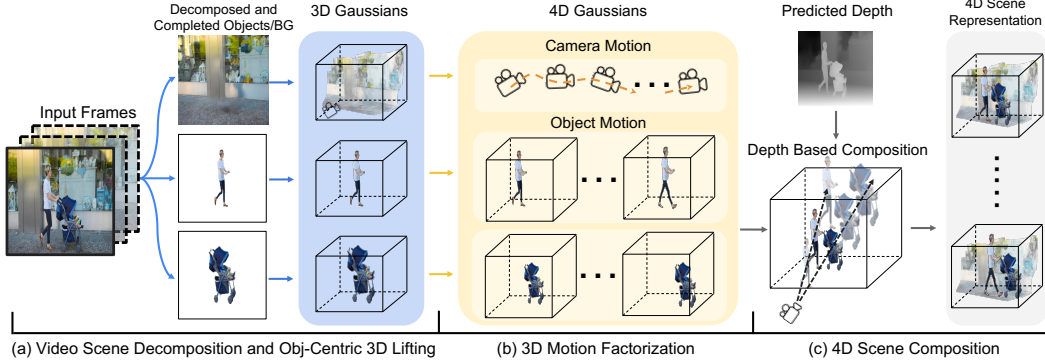


Figure 2: **Method overview for DreamScene4D:** (a) We first decompose and amodally complete each object and the background in the video sequence and use DreamGaussian [48] to obtain static 3D Gaussian representation. (b) Next, we factorize and optimize the motion of each object track independently, detailed in Figure 3. (c) Finally, we use the estimated monocular depth to compose the independently optimized 4D Gaussians into one unified coordinate frame.

motion, represented by a set of camera pose changes. Once optimized, the three components can be composed to form the object dynamics observed in the video.

Object-Centric Motion Optimization The deformation of the 3D Gaussians includes a set of learnable parameters for each Gaussian: **1)** a 3D displacement for each timestep $\mu_t = (\mu_{x_t}, \mu_{y_t}, \mu_{z_t})$, **2)** a 3D rotation for each timestep, represented by a quaternion $\mathcal{R}_t = (qw_t, qx_t, qy_t, qz_t)$, and **3)** a 3D scale for each timestep $s_t = (sx_t, sy_t, sz_t)$. The RGB (spherical harmonics) and opacity of the Gaussians are shared across all timesteps and copied from the first-frame 3D Gaussians.

To compute the 3D object motion in the object-centric frames, we take the cropped and scaled objects in the individual frames I_t , forming a new set of frames \tilde{I}_t^r for each object, where these objects are centered and re-scaled to 65% of the input image. Following [42], we adopt a deformation network $D_\theta(G_0^{obj}, t)$, which consists of a multi-resolution K-Planes [11, 4] and a small MLP. This deformation network predicts the 10-D deformation parameters (μ_t, R_t, s_t) for each object per timestep. We denote the rendered image at timestep t under the camera pose p as $\hat{I}_t^p = \phi(D_\theta(G_0^{obj}, t), p)$. Following [42], we optimize the deformation network using the RGB rendering and SDS loss as:

$$\mathcal{L}_{\text{rgb}}^{\text{video}} = \frac{1}{T} \sum_{t=1}^T \left\| \tilde{I}_t - \hat{I}_t^r \right\|_2^2, \quad (5)$$

$$\nabla_\phi \mathcal{L}_{\text{SDS}}^{\text{video}} = \mathbb{E}_{t, \tau, \epsilon, p} \left[w(\tau) \left(\epsilon_\theta \left(\hat{I}_t^p; \tau, \tilde{I}_t, p \right) - \epsilon \right) \frac{\partial \hat{I}_t^p}{\partial \phi} \right], \quad (6)$$

where $w(\tau)$ is the SDS weighting function, $\epsilon_\theta(\cdot)$ is the predicted noise from a diffusion prior, and ϵ is the added noise. We use the superscript r to denote the reference camera pose corresponding to \tilde{I}_t , and p to represent an arbitrary camera pose.

Since 3D Gaussians can freely move within the uniformly-colored region without penalties, we find that the two losses in Eq. 5 and Eq. 6 are often insufficient for capturing accurate motion, especially for regions with near-uniform colors. Thus, we additionally introduce a flow rendering loss $\mathcal{L}_{\text{flow}}$, which is the masked L1 loss between the rendered optical flow of the Gaussians and the flow predicted by an off-the-shelf optical flow estimator [53]. The flow rendering loss only applies to the confident masked regions that pass a simple forward-backward flow consistency check.

Physical Motion Prior 3D motion in the real world follows a set of physics laws, which can be used to further constrain the Gaussian deformations [29]. The dynamic objects usually maintain a similar size in temporally neighboring frames. Thus, we incorporate the scale regularization loss $\mathcal{L}_{\text{scale}}$ as:

$$\mathcal{L}_{\text{scale}} = \frac{1}{T} \sum_{t=1}^T \|s_{t+1} - s_t\|_1, \quad (7)$$

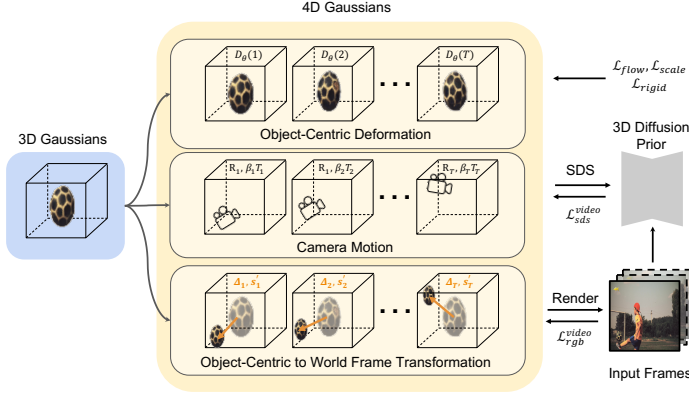


Figure 3: 3D Motion Factorization. The 3D motion is decomposed into 3 components: 1) the object-centric deformation, 2) the camera motion, and 3) the object-centric to-world frame transformation. After optimization, they can be composed to form the original object motion observed in the video.

where we penalize large Gaussian scale changes. To preserve the local rigidity during motion, we penalize changes to relative 3D distance and orientation between neighboring Gaussians using $\mathcal{L}_{\text{rigid}}$:

$$\mathcal{L}_{\text{rigid}} = \frac{1}{|\mathcal{K}|} \sum_{i,j \in \mathcal{K}} w_{i,j} \|(\mu_{j,t-1} - \mu_{i,t-1}) - \mathcal{R}_{i,t-1} \mathcal{R}_{i,t}^{-1} (\mu_{j,t} - \mu_{i,t})\|_2. \quad (8)$$

At timestep t , the local rigidity loss is computed between the 16 nearest neighbors of each Gaussian i with 3D displacement $\mu_{i,t}$ and rotation $\mathcal{R}_{i,t}$. The K-Nearest Neighbors of each Gaussian i are computed in the beginning frame and denoted as set \mathcal{K} . A weighting factor $w_{i,j}$ is applied to the individual loss terms based on the distance between pairs of Gaussians (i, j) :

$$w_{i,j} = \exp\left(-\lambda_w \|\mu_{j,1} - \mu_{i,1}\|_2^2\right), \quad (9)$$

where λ_w is a fixed hyperparameter. The loss imposes additional constraints on the Gaussian deformations, which is especially helpful under self-occlusions where other losses do not provide much information. We disallow pruning and densification of the Gaussians when optimizing for the deformations like [42, 29].

Global Object Motion in the World Frame After obtaining the object-centric motions, we compute the transformation from the object-centric frame to the input world frame. The cropping and scaling operation (Sec 3.2.1) from the original to the object-centric frames can be represented as an affine warp. From this affine warp, we analytically compute a corresponding 3D displacement vector $\Delta_t = (\Delta_{x,t}, \Delta_{y,t}, \Delta_{z,t})$ and a scaling factor s'_t for each object in each frame by setting $\Delta_{z,t} = 0$ that warps the Gaussians from the object-centric frame to the world frame. We then adopt the rendering loss in Eq. 5 on I_t instead of center-cropped frames \tilde{I}_t to fine-tune Δ_t with a low learning rate.

To further improve generation quality, it is essential to consider the perceptual parallax difference. This arises when altering the object’s position in 3D space while maintaining a fixed camera perspective, resulting in subtle changes in rendered object parts. Consequently, we undertake a multi-step optimization approach. Initially, we optimize the three motion components individually. Subsequently, these components are amalgamated, and through a joint optimization process employing Eq. 5, we fine-tune both the deformation network D_θ and affine displacement Δ_t . This refinement process, conducted over a limited number of iterations, helps mitigate the parallax effect.

Camera Motion Estimation To estimate the camera motion from monocular videos, we use the off-the-shelf algorithms [21, 49], to initialize the relative camera pose predictions $\{R_t, T_t\}$ between frame 1 and frame t . However, the camera motion can only be estimated up to an unknown scale [58] as there is no metric depth usage. Therefore, we also estimate a scaling term β for T_t using a rendering or re-projection loss. We first un-project the background points using predicted depth in the first frame, then initialize and optimize the 3D Gaussians of the background using the unprojected point cloud to refine the camera pose estimation. From the background Gaussians G^{bg} and $\{R_t, T_t\}$, we perform a hierarchical grid search over possible values of β to minimize the rendering loss of the background in subsequent frames:

$$\mathcal{L}_\beta = \sum_{t=1}^T \|I_t - \phi(G^{bg}, R_t, \beta T_t)\|_2, \quad (10)$$

Empirically, optimizing a separate β_t per frame [3] yields better results by allowing the renderer to compensate for erroneous camera pose predictions.

3.3 4D Scene Composition with Monocular Depth Guidance

After obtaining the individually optimized 4D Gaussians, we compose them into a unified world coordinate frame to form a coherent 4D scene. This can be achieved by exploiting the relative depth relationships between the objects, as determining the depth of an object in a common 3D coordinate frame also determines its scale.

We take an off-the-shelf depth estimator [55] and compute the depth of each object and the background in the first frame. Next, we randomly pick an object as the “reference” object and estimate the relative depth scales between the reference object and all other objects. The Gaussians are scaled along the camera rays for the given relative scaling factor k . The 3D positions μ'_t and scales s'_t of the scaled Gaussians are described as:

$$\mu'_t = C^r - (C^r - \mu_t) * k, \quad s'_t = s_t * k \quad (11)$$

where C^r represents the position of the camera. Finally, we compose and render the depth map of the reference and scaled object, and compute the affine-invariant L1 loss [55, 41] between the rendered and predicted depth map:

$$\mathcal{L}_{depth} = \frac{1}{HW} \sum_{i=1}^{HW} \left\| \hat{d}_i^* - \hat{d}_i \right\|_1, \quad \hat{d}_i = \frac{d_i - t(d)}{\sigma(d)}. \quad (12)$$

Here, \hat{d}_i^* and \hat{d}_i are the scaled and shifted versions of the rendered depth d_i^* and predicted depth d_i . $t(d)$ is defined as the reference object’s median depth and $\sigma(d)$ is defined as the difference between the 90% and 10% quantile of the reference object. The two depth maps are normalized separately using their own $t(d)$ and $\sigma(d)$. Finally, we place and re-compose the individual objects back into a common coordinate frame by minimizing this loss for each object w.r.t. to the chosen reference object (e.g. using grid search in Section 3.2.2). These Gaussians can then be rendered jointly to form a scene-level 4D representation.

4 Experiments

Datasets We evaluate the performance of DreamScene4D on multiple popular and challenging video datasets, including DAVIS [36], Kubric [13], and some self-captured videos. For the video-to-4D task, we evaluate using a subset of 30 real-world challenging DAVIS [36] videos, consisting of multi-object monocular videos with various amounts of motion in the real world. We further incorporate the labeled point trajectories in 10 videos from TAP-Vid-DAVIS [9] to evaluate the accuracy of the learned Gaussian deformations. In addition, we generated 50 multi-object videos from the Kubric [13] simulator, which provides challenging scenarios where objects can be small or very off-center. To ablate our extensions to SD-Inpaint for video amodal completion, we randomly select 120 videos from YoutubeVOS [54] and generate random occlusion masks in the video [47, 7].

Evaluation Metrics The quality of 4D generation can be measured in two aspects: the view rendering quality of the reconstructed 3D geometry of the scene, and the accuracy of the 3D motion. For the former, we follow previous works [15, 42] and report the CLIP [40] and LPIPS [62] scores between 4 novel-view rendered frames and the reference frame, and compute its average score per video. These metrics allow us to assess the semantic similarity between rendered and reference frames.

The accuracy of the estimated motion can be benchmarked using 2D point trajectory annotations from TAP-Vid-DAVIS and Kubric by measuring the End Point Error (EPE). Thus, for Kubric, we also report the mean EPE separately for fully visible points and points that undergo occlusion. For DAVIS, we report the mean and median EPE [64], as the annotations only exist for visible points.

For video amodal completion, we follow inpainting works [47, 7] and report the overall PSNR, the PSNR in the masked region, and perceptual scores such as LPIPS and Temporal Consistency (TC) [6].

Implementation Details We run our experiments on one 40GB A100 GPU. We crop and scale the individual objects to around 65% of the image size for object lifting. For static 3D Gaussian optimization, we optimize for 1000 iterations with a batch size of 16 for 5 minutes. For optimizing

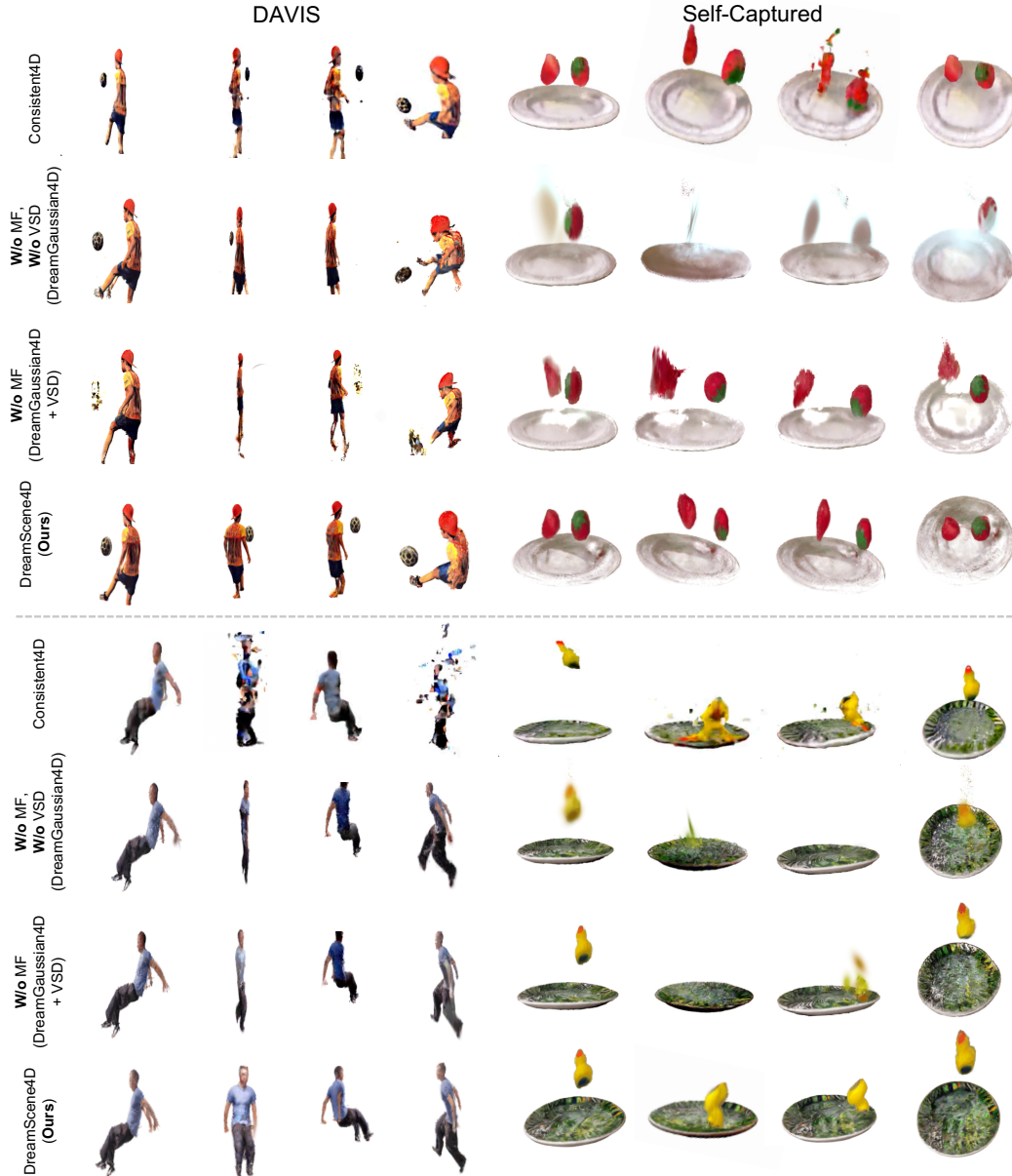


Figure 4: **Video to 4D Comparisons.** We render the Gaussians at various timesteps and camera views. We denote Motion Factorization as **MF** and Video Scene Decomposition as **VSD**. Our method produces consistent and faithful renders for fast-moving objects, while DreamGaussian4D [42] and Consistent4D [15] produce distorted 3D geometry, blurring, or broken artifacts.

the dynamic components, we optimize for 10 times the number of frames with a batch size of 10. More implementation details are provided in the supplemental file.

4.1 Video to 4D Scene Generation

Baselines For video-to-4D scene generation, we consider DreamGaussian4D [42] as the baseline, which also uses dynamic Gaussian Splatting for its 4D scene representation. We replace the frames generated from image-to-video models in DreamGaussian4D with the reference frames from videos. As the baseline DreamGaussian4D mainly handles single-object videos, we additionally compare against its variant where we combined DreamGaussian4D with Video Scene Decomposition (VSD) (Section 3.1), then recomposed those object Gaussians. We also perform ablation experiments where we remove the flow rendering loss and the physics-based motion losses.

Table 1: **4D Generation Quality Comparisons.** We report the CLIP score, LPIPS in Kubric [13] and DAVIS [36]. We denote methods with Video Scene Decomposition as **VSD** and methods with Motion Factorization as **MF**.

Method	VSD	MF	DAVIS		Kubric	
			CLIP \uparrow	LPIPS \downarrow	CLIP \uparrow	LPIPS \downarrow
Baseline: DreamGaussian4D [42]	\times	\times	77.81	0.181	73.45	0.146
w/ VSD	\checkmark	\times	81.39	0.169	79.83	0.122
DreamScene4D (Ours)	\checkmark	\checkmark	85.09	0.152	85.53	0.112
w/o \mathcal{L}_{flow}	\checkmark	\checkmark	84.94	0.152	86.41	0.113
w/o \mathcal{L}_{rigid} and \mathcal{L}_{scale}	\checkmark	\checkmark	83.24	0.153	84.07	0.115

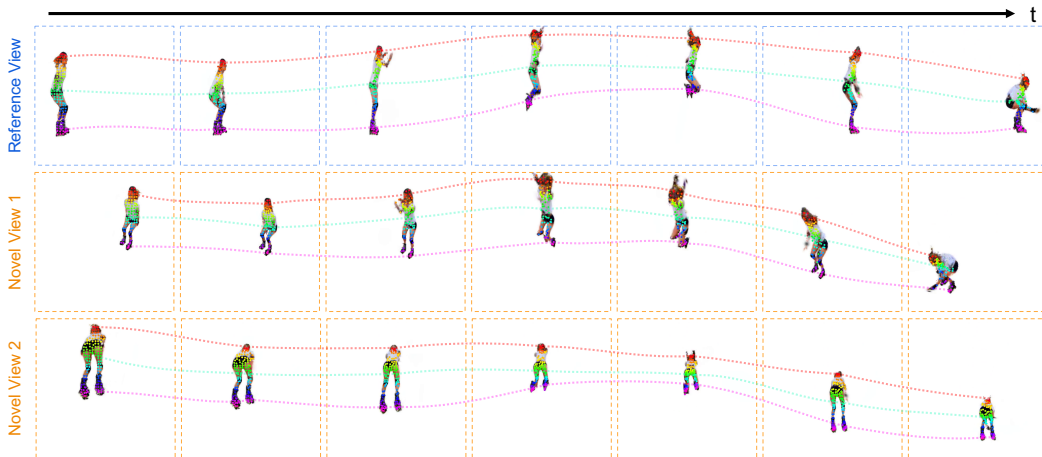


Figure 5: **Gaussian Motion Visualizations.** We visualize the Gaussian trajectories in the reference view corresponding to the video as well in multiple novel views. The rendered Gaussians are sampled *independently* for each view. DreamScene4D can produce accurate motion in different camera poses *w/o* explicit point trajectory supervision.

4D Generation Results on DAVIS & Kubric We present the 4D generation quality comparison in Table 1, where our proposed Video Scene Decomposition (VSD) and Motion Factorization (MF) schemes greatly improve the CLIP and LPIPS score compared to the input reference images. We also show qualitative comparisons of 4D generation on multi-object videos and videos with large motion in Figure 4, where both variants of DreamGaussian4D [42] and Consistent4D [15] tend to produce distorted 3D geometry, faulty motion, or broken artifacts of objects. This highlights the applicability of DreamScene4D to handle more complex videos captured in the real world.

4D Generation Results on Self-Captured Videos We also captured some monocular videos with fast object motion using a smartphone to test the robustness of DreamScene4D, where objects can be off-center and are subject to motion blur. We present qualitative results of the rendered 4D Gaussians in the right half of Figure 4. Even under more casual video capturing settings with large motion blur, DreamScene4D can still provide temporally consistent 4D scene generation results. At the same time, the baselines generate blurry results or contain broken artifacts of the objects.

4.2 4D Gaussian Motion Accuracy

Baselines To evaluate the accuracy of the 4D Gaussian motion, we consider DreamGaussian4D [42] as the baseline, since extracting motion from NeRF-based methods [15] is highly non-trivial. In addition, we compare against PIPS++ [64] and CoTracker [16], two fully-supervised methods explicitly trained for point-tracking, serving as upper bounds for performance.

4D Motion Accuracy in Video Reference Views In Table 2, we tabulate the motion accuracy comparison, where DreamScene4D achieves significantly lower EPE than the baseline DreamGaussian4D on both the DAVIS and Kubric datasets. We noted that conventional baselines often fail when objects



Figure 6: **Motion Comparisons.** The 2D projected motion of Gaussians accurately aligns with dynamic human motion trajectory in the video, where the point trajectories estimated by PIPS++ [64] tend to get “stuck” in the background wall. For CoTracker [16], partial point trajectories are mixed up, where some points in the chest region (yellow/green) ending up in the head area (red).

Table 2: **Gaussian Motion Accuracy.** We report the EPE in Kubric [13] and DAVIS [36, 9]. We denote methods with our Video Scene Decomposition in column **VSD** and methods with 3D Motion Factorization in column **MF**. Note that CoTracker is trained on Kubric.

Method	VSD	MF	DAVIS		Kubric		
			EPE (vis) ↓	EPE (occ) ↓	Mean EPE ↓	Median EPE ↓	
<i>(a) Not trained on point tracking data</i>							
Baseline: DreamGaussian4D [42]	✗	✗	26.65	6.98	101.79	120.95	
w/ VSD	✓	✗	20.95	6.72	85.27	92.42	
DreamScene4D (Ours)	✓	✓	8.56	4.24	14.30	18.31	
w/o \mathcal{L}_{flow}	✓	✓	10.91	3.83	18.54	24.51	
w/o \mathcal{L}_{rigid} and \mathcal{L}_{scale}	✓	✓	10.29	4.78	16.21	22.29	
<i>(b) Trained on point tracking data</i>							
PIPS++ [64]	-	-	19.61	5.36	16.72	29.65	
CoTracker [16]	-	-	7.20	2.08	2.51	6.75	

are positioned near the edges of the video frame or undergo large motion. In contrast, thanks to motion factorization, DreamScene4D remains largely robust under such conditions, as we perform the deformation optimizations in an object-centric frame instead of directly in the global frame. Interestingly, the motion accuracy of DreamScene4D outperforms PIPS++ [64], despite never being trained for point tracking. This is due to the strong object priors of DreamScene4D, as the Gaussians adhere to remaining on the same object it generates and their motion is often strongly correlated. In contrast, the tracking in PIPS++ is unconstrained, where the motion of the points gets “stuck” on other objects or the background when large movements occur, as shown in Figure 6.

4D Motion Results on Generated Novel Views An advantage of representing the scene using 4D Gaussians is being able to obtain motion trajectories for arbitrary camera poses, which we visualize in Figure 5. DreamScene4D can both generate a 4D scene with consistent appearance across views and produce temporally coherent motion trajectories in novel views from monocular inputs.

4.3 Video Amodal Completion

We compare against Repaint [28] and SD-Inpaint [44] for video amodal completion. Both baseline methods are based on Stable Diffusion. Repaint alters the reverse diffusion iterations by sampling the unmasked regions of the image. SD-Inpaint, on the other hand, finetunes Stable Diffusion for free-form inpainting. We also ablate the performance of our proposed amodal completion approach without the inflated spatiotemporal self-attention (denoted as STSA) and consistency guidance in Sec. 3.1. We summarize the results in Table 3 and show qualitative samples in the supplemental file. DreamScene4D achieves more consistent and accurate video completion than the image inpainting approaches, by leveraging temporal information during the denoising process. Note that these techniques complement other video completion approaches since DreamScene4D mainly focuses on video-to-4D scene generation.

Table 3: **Video Amodal Completion Evaluations.** We report the PSNR, LPIPS, and Temporal Consistency (TC) measured using CLIP similarity in randomly masked YoutubeVOS [54] videos.

Method	PSNR \uparrow	PSNR \uparrow (masked)	LPIPS \downarrow	TC \uparrow
Repaint [28]	20.76	14.04	0.23	91.18
SD-Inpaint [44]	21.07	14.35	0.23	91.72
DreamScene4D (Ours)	22.27	16.09	0.22	93.40
w/o STSA	21.56	15.31	0.23	92.58
w/o Guidance	21.71	15.20	0.23	92.91

4.4 Limitations

Despite the exciting progress and results presented in the paper, several limitations still exist: **(1)** The 3D diffusion prior fails to generalize to videos captured from a camera with steep elevation angles. **(2)** Scene composition may fall into local suboptimas if the rendered depth of the lifted 3D objects is not well aligned with the estimated depth. **(3)** Despite the inpainting, the Gaussians are still under-constrained when heavy occlusions happen, and artifacts may occur. We hope to improve our proposed approach for these cases in the future.

5 Conclusion

We propose DreamScene4D, the first video-to-4D scene generation work to take complex multi-object videos as input and generate dynamic 3D scenes across occlusions, large object motions, and unseen viewpoints with both temporal and spatial consistency. This is achieved by decomposing the video scene into the background and individual object trajectories, along with a motion factorization scheme to handle fast-moving objects in multi-object scenes. We present arbitrary novel view generation results of DreamScene4D on popular video datasets like DAVIS, Kubric, and challenging self-captured videos. In addition, DreamScene4D not only achieves accurate Gaussian motion in the visible reference view but also enables robust motion tracking in the synthesized novel views.

Acknowledgments and Disclosure of Funding

This research was supported by Toyota Research Institute.

References

- [1] Sherwin Bahmani, Xian Liu, Yifan Wang, Ivan Skorokhodov, Victor Rong, Ziwei Liu, Xihui Liu, Jeong Joon Park, Sergey Tulyakov, Gordon Wetzstein, et al. Tc4d: Trajectory-conditioned text-to-4d generation. *arXiv preprint arXiv:2403.17920*, 2024.
- [2] Sherwin Bahmani, Ivan Skorokhodov, Victor Rong, Gordon Wetzstein, Leonidas Guibas, Peter Wonka, Sergey Tulyakov, Jeong Joon Park, Andrea Tagliasacchi, and David B Lindell. 4d-fy: Text-to-4d generation using hybrid score distillation sampling. *arXiv preprint arXiv:2311.17984*, 2023.
- [3] Wenjing Bian, Zirui Wang, Kejie Li, Jia-Wang Bian, and Victor Adrian Prisacariu. Nope-nerf: Optimising neural radiance field with no pose prior. In *CVPR*, 2023.
- [4] Ang Cao and Justin Johnson. Hexplane: A fast representation for dynamic scenes. In *CVPR*, 2023.
- [5] Duygu Ceylan, Chun-Hao P Huang, and Niloy J Mitra. Pix2video: Video editing using image diffusion. In *ICCV*, 2023.
- [6] Wenhao Chai, Xun Guo, Gaoang Wang, and Yan Lu. Stablevideo: Text-driven consistency-aware diffusion video editing. In *ICCV*, 2023.
- [7] Ya-Liang Chang, Zhe Yu Liu, Kuan-Ying Lee, and Winston Hsu. Learnable gated temporal shift module for deep video inpainting. *BMVC*, 2019.
- [8] Ho Kei Cheng and Alexander G Schwing. Xmem: Long-term video object segmentation with an atkinson-shiffrin memory model. In *ECCV*, 2022.
- [9] Carl Doersch, Ankush Gupta, Larisa Markeeva, Adria Recasens, Lucas Smaira, Yusuf Aytar, Joao Carreira, Andrew Zisserman, and Yi Yang. Tap-vid: A benchmark for tracking any point in a video. In *NeurIPS*, 2022.
- [10] Kiana Ehsani, Roozbeh Mottaghi, and Ali Farhadi. Segan: Segmenting and generating the invisible. In *CVPR*, 2018.
- [11] Sara Fridovich-Keil, Giacomo Meanti, Frederik Rahbæk Warburg, Benjamin Recht, and Angjoo Kanazawa. K-planes: Explicit radiance fields in space, time, and appearance. In *CVPR*, 2023.
- [12] Quankai Gao, Qiangeng Xu, Zhe Cao, Ben Mildenhall, Wenchao Ma, Le Chen, Danhang Tang, and Ulrich Neumann. Gaussianflow: Splatting gaussian dynamics for 4d content creation. *arXiv preprint arXiv:2403.12365*, 2024.
- [13] Klaus Greff, Francois Belletti, Lucas Beyer, Carl Doersch, Yilun Du, Daniel Duckworth, David J Fleet, Dan Gnanapragasam, Florian Golemo, Charles Herrmann, et al. Kubric: A scalable dataset generator. In *CVPR*, 2022.
- [14] Eric Heiden, Ziang Liu, Vibhav Vineet, Erwin Coumans, and Gaurav S Sukhatme. Inferring articulated rigid body dynamics from rgb-d video. In *IROS*, 2022.
- [15] Yanqin Jiang, Li Zhang, Jin Gao, Weimin Hu, and Yao Yao. Consistent4d: Consistent 360 $\{\deg\}$ dynamic object generation from monocular video. *arXiv preprint arXiv:2311.02848*, 2023.
- [16] Nikita Karaev, Ignacio Rocco, Benjamin Graham, Natalia Neverova, Andrea Vedaldi, and Christian Rupprecht. Cotracker: It is better to track together. *arXiv preprint arXiv:2307.07635*, 2023.
- [17] Lei Ke, Yu-Wing Tai, and Chi-Keung Tang. Occlusion-aware video object inpainting. In *ICCV*, 2021.
- [18] Lei Ke, Mingqiao Ye, Martin Danelljan, Yifan Liu, Yu-Wing Tai, Chi-Keung Tang, and Fisher Yu. Segment anything in high quality. In *NeurIPS*, 2023.
- [19] Bernhard Kerbl, Georgios Kopanas, Thomas Leimkühler, and George Drettakis. 3d gaussian splatting for real-time radiance field rendering. *ACM Transactions on Graphics*, 42(4):1–14, 2023.
- [20] Levon Khachatryan, Andranik Movsisyan, Vahram Tadevosyan, Roberto Henschel, Zhangyang Wang, Shant Navasardyan, and Humphrey Shi. Text2video-zero: Text-to-image diffusion models are zero-shot video generators. In *ICCV*, 2023.
- [21] Johannes Kopf, Xuejian Rong, and Jia-Bin Huang. Robust consistent video depth estimation. In *CVPR*, 2021.
- [22] Yuseung Lee, Kunho Kim, Hyunjin Kim, and Minhyuk Sung. Syncdiffusion: Coherent montage via synchronized joint diffusions. *NeurIPS*, 2023.
- [23] Tianye Li, Mira Slavcheva, Michael Zollhoefer, Simon Green, Christoph Lassner, Changil Kim, Tanner Schmidt, Steven Lovegrove, Michael Goesele, Richard Newcombe, et al. Neural 3d video synthesis from multi-view video. In *CVPR*, 2022.
- [24] Huan Ling, Seung Wook Kim, Antonio Torralba, Sanja Fidler, and Karsten Kreis. Align your gaussians: Text-to-4d with dynamic 3d gaussians and composed diffusion models. *arXiv preprint arXiv:2312.13763*, 2023.
- [25] Lingjie Liu, Jiatao Gu, Kyaw Zaw Lin, Tat-Seng Chua, and Christian Theobalt. Neural sparse voxel fields. *Advances in Neural Information Processing Systems*, 33:15651–15663, 2020.
- [26] Ruoshi Liu, Rundi Wu, Basile Van Hoorick, Pavel Tokmakov, Sergey Zakharov, and Carl Vondrick. Zero-1-to-3: Zero-shot one image to 3d object. In *ICCV*, 2023.
- [27] Stephen Lombardi, Tomas Simon, Jason Saragih, Gabriel Schwartz, Andreas Lehrmann, and Yaser Sheikh. Neural volumes: Learning dynamic renderable volumes from images. *arXiv preprint arXiv:1906.07751*, 2019.

- [28] Andreas Lugmayr, Martin Danelljan, Andres Romero, Fisher Yu, Radu Timofte, and Luc Van Gool. Repaint: Inpainting using denoising diffusion probabilistic models. In *CVPR*, 2022.
- [29] Jonathon Luiten, Georgios Kopanas, Bastian Leibe, and Deva Ramanan. Dynamic 3d gaussians: Tracking by persistent dynamic view synthesis. In *3DV*, 2024.
- [30] Ben Mildenhall, Pratul P. Srinivasan, Matthew Tancik, Jonathan T. Barron, Ravi Ramamoorthi, and Ren Ng. Nerf: Representing scenes as neural radiance fields for view synthesis. In *ECCV*, 2020.
- [31] Zijie Pan, Zeyu Yang, Xiatian Zhu, and Li Zhang. Fast dynamic 3d object generation from a single-view video. *arXiv preprint arXiv:2401.08742*, 2024.
- [32] Keunhong Park, Utkarsh Sinha, Jonathan T Barron, Sofien Bouaziz, Dan B Goldman, Steven M Seitz, and Ricardo Martin-Brualla. Nerfies: Deformable neural radiance fields. In *ICCV*, 2021.
- [33] Keunhong Park, Utkarsh Sinha, Peter Hedman, Jonathan T. Barron, Sofien Bouaziz, Dan B Goldman, Ricardo Martin-Brualla, and Steven M. Seitz. Hypernerf: A higher-dimensional representation for topologically varying neural radiance fields. *ACM Trans. Graph.*, 40(6), dec 2021.
- [34] Gaurav Parmar, Krishna Kumar Singh, Richard Zhang, Yijun Li, Jingwan Lu, and Jun-Yan Zhu. Zero-shot image-to-image translation. In *SIGGRAPH*, 2023.
- [35] Xue Bin Peng, Angjoo Kanazawa, Jitendra Malik, Pieter Abbeel, and Sergey Levine. Sfv: Reinforcement learning of physical skills from videos. *ACM Transactions On Graphics (TOG)*, 37(6):1–14, 2018.
- [36] Jordi Pont-Tuset, Federico Perazzi, Sergi Caelles, Pablo Arbeláez, Alex Sorkine-Hornung, and Luc Van Gool. The 2017 davis challenge on video object segmentation. *arXiv preprint arXiv:1704.00675*, 2017.
- [37] Ben Poole, Ajay Jain, Jonathan T Barron, and Ben Mildenhall. Dreamfusion: Text-to-3d using 2d diffusion. *ICLR*, 2023.
- [38] Albert Pumarola, Enric Corona, Gerard Pons-Moll, and Francesc Moreno-Noguer. D-nerf: Neural radiance fields for dynamic scenes. In *CVPR*, 2021.
- [39] Chenyang Qi, Xiaodong Cun, Yong Zhang, Chenyang Lei, Xintao Wang, Ying Shan, and Qifeng Chen. Fatezero: Fusing attentions for zero-shot text-based video editing. In *ICCV*, 2023.
- [40] Alec Radford, Jong Wook Kim, Chris Hallacy, Aditya Ramesh, Gabriel Goh, Sandhini Agarwal, Girish Sastry, Amanda Askell, Pamela Mishkin, Jack Clark, et al. Learning transferable visual models from natural language supervision. In *ICML*, 2021.
- [41] René Ranftl, Katrin Lasinger, David Hafner, Konrad Schindler, and Vladlen Koltun. Towards robust monocular depth estimation: Mixing datasets for zero-shot cross-dataset transfer. *TPAMI*, 44(3), 2022.
- [42] Jiawei Ren, Liang Pan, Jiayang Tang, Chi Zhang, Ang Cao, Gang Zeng, and Ziwei Liu. Dreamgaussian4d: Generative 4d gaussian splatting. *arXiv preprint arXiv:2312.17142*, 2023.
- [43] Tianhe Ren, Shilong Liu, Ailing Zeng, Jing Lin, Kunchang Li, He Cao, Jiayu Chen, Xinyu Huang, Yukang Chen, Feng Yan, et al. Grounded sam: Assembling open-world models for diverse visual tasks. *arXiv preprint arXiv:2401.14159*, 2024.
- [44] Robin Rombach, Andreas Blattmann, Dominik Lorenz, Patrick Esser, and Björn Ommer. High-resolution image synthesis with latent diffusion models. In *CVPR*, 2022.
- [45] Uriel Singer, Shelly Sheynin, Adam Polyak, Oron Ashual, Iurii Makarov, Filippos Kokkinos, Naman Goyal, Andrea Vedaldi, Devi Parikh, Justin Johnson, et al. Text-to-4d dynamic scene generation. *arXiv preprint arXiv:2301.11280*, 2023.
- [46] Jiaming Song, Chenlin Meng, and Stefano Ermon. Denoising diffusion implicit models. *ICLR*, 2021.
- [47] Roman Suvorov, Elizaveta Logacheva, Anton Mashikhin, Anastasia Remizova, Arsenii Ashukha, Aleksei Silvestrov, Naejin Kong, Harshith Goka, Kiwoong Park, and Victor Lempitsky. Resolution-robust large mask inpainting with fourier convolutions. In *WACV*, 2022.
- [48] Jiayang Tang, Jiawei Ren, Hang Zhou, Ziwei Liu, and Gang Zeng. Dreamgaussian: Generative gaussian splatting for efficient 3d content creation. *ICLR*, 2024.
- [49] Shuzhe Wang, Vincent Leroy, Yohann Cabon, Boris Chidlovskii, and Jerome Revaud. Dust3r: Geometric 3d vision made easy. In *CVPR*, 2024.
- [50] Guanjun Wu, Taoran Yi, Jiemin Fang, Lingxi Xie, Xiaopeng Zhang, Wei Wei, Wenyu Liu, Qi Tian, and Xinggang Wang. 4d gaussian splatting for real-time dynamic scene rendering. In *CVPR*, 2024.
- [51] Jay Zhangjie Wu, Yixiao Ge, Xintao Wang, Stan Weixian Lei, Yuchao Gu, Yufei Shi, Wynne Hsu, Ying Shan, Xiaohu Qie, and Mike Zheng Shou. Tune-a-video: One-shot tuning of image diffusion models for text-to-video generation. In *ICCV*, 2023.
- [52] Dejia Xu, Hanwen Liang, Neel P Bhatt, Hezhen Hu, Hanxue Liang, Konstantinos N Plataniotis, and Zhangyang Wang. Comp4d: Llm-guided compositional 4d scene generation. *arXiv preprint arXiv:2403.16993*, 2024.
- [53] Haofei Xu, Jing Zhang, Jianfei Cai, Hamid Rezaatofghi, and Dacheng Tao. Gmflow: Learning optical flow via global matching. In *CVPR*, 2022.
- [54] Ning Xu, Linjie Yang, Yuchen Fan, Jianchao Yang, Dingcheng Yue, Yuchen Liang, Brian Price, Scott Cohen, and Thomas Huang. Youtube-vos: Sequence-to-sequence video object segmentation. In *ECCV*, 2018.

- [55] Lihe Yang, Bingyi Kang, Zilong Huang, Xiaogang Xu, Jiashi Feng, and Hengshuang Zhao. Depth anything: Unleashing the power of large-scale unlabeled data. In *CVPR*, 2024.
- [56] Qitong Yang, Mingtao Feng, Zijie Wu, Shijie Sun, Weisheng Dong, Yaonan Wang, and Ajmal Mian. Beyond skeletons: Integrative latent mapping for coherent 4d sequence generation. *arXiv preprint arXiv:2403.13238*, 2024.
- [57] Ziyi Yang, Xinyu Gao, Wen Zhou, Shaohui Jiao, Yuqing Zhang, and Xiaogang Jin. Deformable 3d gaussians for high-fidelity monocular dynamic scene reconstruction. *arXiv preprint arXiv:2309.13101*, 2023.
- [58] Vickie Ye, Georgios Pavlakos, Jitendra Malik, and Angjoo Kanazawa. Decoupling human and camera motion from videos in the wild. In *CVPR*, 2023.
- [59] Yuyang Yin, Dejie Xu, Zhangyang Wang, Yao Zhao, and Yunchao Wei. 4dgen: Grounded 4d content generation with spatial-temporal consistency. *arXiv preprint arXiv:2312.17225*, 2023.
- [60] Yifei Zeng, Yanqin Jiang, Siyu Zhu, Yuanxun Lu, Youtian Lin, Hao Zhu, Weiming Hu, Xun Cao, and Yao Yao. Stag4d: Spatial-temporal anchored generative 4d gaussians. *arXiv preprint arXiv:2403.14939*, 2024.
- [61] Xiaohang Zhan, Xingang Pan, Bo Dai, Ziwei Liu, Dahua Lin, and Chen Change Loy. Self-supervised scene de-occlusion. In *CVPR*, 2020.
- [62] Richard Zhang, Phillip Isola, Alexei A Efros, Eli Shechtman, and Oliver Wang. The unreasonable effectiveness of deep features as a perceptual metric. In *CVPR*, 2018.
- [63] Yuyang Zhao, Zhiwen Yan, Enze Xie, Lanqing Hong, Zhenguo Li, and Gim Hee Lee. Animate124: Animating one image to 4d dynamic scene. *arXiv preprint arXiv:2311.14603*, 2023.
- [64] Yang Zheng, Adam W Harley, Bokui Shen, Gordon Wetzstein, and Leonidas J Guibas. Pointodyssey: A large-scale synthetic dataset for long-term point tracking. In *ICCV*, 2023.
- [65] Yufeng Zheng, Xueting Li, Koki Nagano, Sifei Liu, Otmar Hilliges, and Shalini De Mello. A unified approach for text-and image-guided 4d scene generation. *arXiv preprint arXiv:2311.16854*, 2023.
- [66] Shangchen Zhou, Chongyi Li, Kelvin CK Chan, and Chen Change Loy. Propainter: Improving propagation and transformer for video inpainting. In *ICCV*, 2023.